PCCP

Dynamics of the Cl + H_2/D_2 reaction: a comparison of crossed molecular beam experiments with quasiclassical trajectory and quantum mechanical calculations

Michele Alagia,†[a] Nadia Balucani,[a] Laura Cartechini,[a] Piergiorgio Casavecchia,*[a] Gian Gualberto Volpi,[a] F. Javier Aoiz,*[b] Luis Bañares,[b] Thomas C. Allison,[c] Steven L. Mielke[c] and Donald G. Truhlar*[c]

[a] *Dipartimento di Chimica, Università di Perugia, 06123 Perugia, Italy. E-mail: piero@dyn.unipg.it*
[b] *Departmento de Química Física, Facultad de Química, Universidad Complutense, 28040 Madrid, Spain*
[c] *Department of Chemistry, Chemical Physics Program, and Supercomputer Institute, University of Minnesota, Minneapolis, MN 55455-0431, USA*

Received 5th November 1999, Accepted 17th December 1999

In this paper we report angular distributions and time-of-flight spectra for the Cl + H_2 → HCl + H and Cl + D_2 → DCl + D reactions at 5.85 kcal mol^{-1} and 6.3 and 6.4 kcal mol^{-1} collision energies, respectively, obtained from high-resolution crossed molecular beam experiments. In addition, quasiclassical trajectory (QCT) and quantum mechanical (QM) dynamical calculations have been carried out for these reactions on the G3 potential energy surface (T. C. Allison *et al.*, *J. Phys. Chem.*, 1996, **100**, 13575). Reaction probabilities, integral and differential cross sections have been calculated using the QCT and QM methodologies, and a comparison of these results is presented. The molecular beam results have been simulated using the theoretical calculations, and theory and experiment are in reasonably good agreement.

I. Introduction

The reactions of chlorine atoms with molecular hydrogen and its isotopomers have received considerable attention both experimentally and theoretically.[1–25] The interest of chemical kineticists in this system goes back to the nineteenth century when it was studied by Draper (1843), Bunsen and Roscoe (1862) and van't Hoff. Later work on this reaction includes the pioneering studies of Chapman, Bodenstein, and Nernst and their collaborators,[7] in connection with the mechanism of the H_2–Cl_2 chain reaction, for which the Cl(^{2}P) + H_2 → HCl + H reaction is the rate-determining step. This reaction has played a central role in fundamental chemical kinetics and has served as a critical test case for bimolecular reaction rate theory, especially transition state and kinetic isotopic effect theories.[8] Besides its fundamental interest, the Cl + H_2 reaction is a prototype for a host of Cl reactions that are important in atmospheric chemistry and for photochemical air pollution. Experimental work on the rate constants of the Cl + H_2 reaction and their temperature dependence is very extensive and has been summarised by Michael and co-workers.[9] Measurements of absolute rate constants[20] for Cl + HD were also reported very recently.

The Cl + H_2 → HCl + H reaction and its isotopic variant Cl + D_2 → DCl + D are nearly thermoneutral ($\Delta H_0^\circ = 1.03$ kcal mol^{-1} and $\Delta H_0^\circ = 1.64$ kcal mol^{-1}, respectively), and the HCl/DCl product can only be formed in the ground vibrational level at low collision energies. The energetics of the reactions are shown in Figs. 1(a) and 1(b) where the spin–orbit levels of chlorine and the rovibrational levels of HCl/DCl products are also indicated.

Reactive cross sections were not available until recently. The molecular products can be conveniently detected by a mass spectrometer in a crossed molecular beam (CMB) experiment, although this is challenging because of a high barrier, a near mass conflict of the product with the second most abundant ^{37}Cl isotope, and particularly unfavourable kinematics. A first account of crossed beam studies of the Cl + H_2 reaction has been reported by the present authors.[3] Measurements of the excitation functions[10] and double (angle and velocity) differential cross sections[11] have been very recently carried out by REMPI detection of the H atoms and Doppler-selected time-of-flight technique in pulsed CMB experiments. Absolute reactive cross sections have been determined for the reverse H + HCl reaction in several laboratories using pump–probe techniques.[21]

As the quality and quantity of experimental data have improved, the quality of potential energy surfaces for the H_2Cl system has improved as well. As a consequence, the H_2Cl system may now be considered a critical test system for the comparison of experimental and theoretical studies, joining the H_3 and H_2F systems as testing grounds for the most detailed and most accurate methods.[6]

A refined potential energy surface (PES) for the H_2Cl system was introduced by two of the authors and co-workers,[12] and it was denoted G3 (see Fig. 1(c)). The G3 PES was based on the GQQ PES of Schwenke *et al.*,[13] which was, in turn, based on the empirical GSW surface of Stern, Persky, and Klein.[14] The partly *ab initio* G3 surface has the advantage over the former GSW and GQQ surfaces that the Cl–H–H bending potential is more accurate along the reaction path. The G3 PES is the most accurate surface currently available for the H_2Cl system, and we have used it for the theoretical dynamics calculations presented here.

† Present address: INFM, Sincrotrone Elettra, 34012 Trieste, Italy.

DOI: 10.1039/a908829f

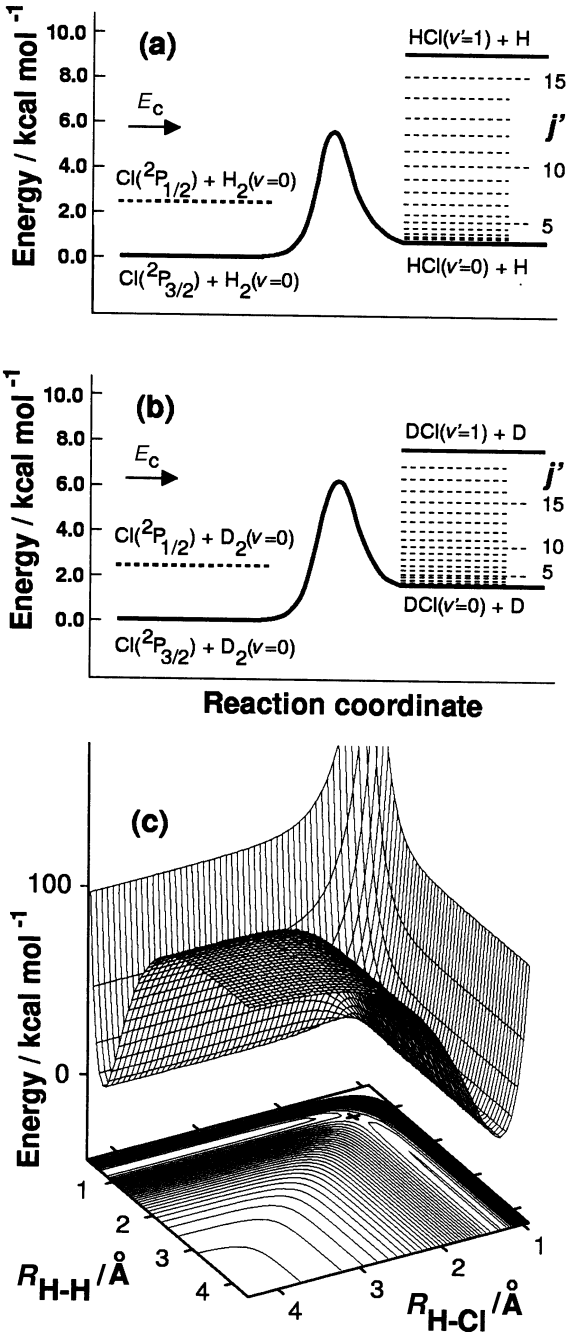

Fig. 1 Energy level and correlation diagram for (a) the $Cl + H_2$ reaction and (b) the $Cl + D_2$ reaction with the spin–orbit levels of atomic chlorine and the rovibrational levels of the products indicated. The effective ground state potential energy barriers of the G3 surface, including zero-point energy for reactant, product and modes transverse to reaction coordinate, are shown as solid curves. The collision energies of the experiments, E_c, are indicated as arrows. (c) Contour map and three-dimensional perspective plot of the G3 PES for the collinear Cl–H–H arrangement. The saddle point (of height 7.88 kcal mol^{-1}) is denoted by an X and R_{H-H} and R_{H-Cl} denote the distances between the specified atoms.

The G3 surface has already been used for a number of dynamical studies. Rate constants for the $Cl + H_2$ and $Cl + D_2$ reactions were computed using variational transition state theory[1,12] (VTST), quantum mechanical[15,16] (QM) dynamic and quasiclassical trajectory[17] (QCT) methods. QCT calculations of differential cross sections for the heteronuclear $Cl + HD(v = 0, 1) \rightarrow HCl(DCl) + D(H)$ reaction are available,[18] and a comparison between QM and QCT calculations and experimental results from a high-resolution molecular beam experiment for the $Cl + H_2$ reaction[3] has been published. Quantized transition states have also been analyzed for the H_2Cl system.[1,19] Accurate quantal differential cross sections (DCS) for the GQQ surface have been reported by Launay *et al.*[22] for the $Cl + H_2(v = 0, j = 0)$ reaction (where v and j denote vibrational and rotational quantum numbers respectively), as well as for the $HCl(v = 0, j = 0–2) + H$ reaction.[23] Accurate quantal results for the $Cl + H_2$ and Cl + HD reactions with total angular momentum J equal to 0 were computed for the GQQ and GSW surfaces by Takada *et al.*,[24] who also reported approximate cross sections and thermal rate constants obtained by the constant centrifugal potential approximation (CCPA). More recently, cross section calculations were reported for the G3 surface.[1,3]

In this paper we present the results of high resolution crossed molecular beam experiments in the form of laboratory angular distributions and time-of-flight spectra at collision energies, E_c, of about 6 kcal mol^{-1} for the reactions

$$Cl(^2P_{3/2,\,1/2}) + \text{n-}H_2(v = 0, j = 0, 1, 2, 3) \rightarrow HCl(v' = 0, \text{all } j') + H$$

$$Cl(^2P_{3/2,\,1/2}) + \text{n-}D_2(v = 0, j = 0, 1, 2, 3, 4) \rightarrow DCl(v' = 0, \text{all } j') + D$$

(In this paper, E_c always denotes *relative* translational energy.) The experimental work is accompanied by scattering calculations of state-to-state ($v, j \rightarrow v', j'$) differential cross sections (DCSs) based on accurate quantum mechanical dynamics as well as the quasiclassical trajectory method, in both cases using the G3 PES. The theoretical DCSs, after transformation into the laboratory frame and averaging over experimental conditions, are compared directly with the laboratory data, thus providing an unambiguous test of the ground-electronic-state PES of $Cl + H_2$.

In addition, since there are only a small number of systems for which both accurate quantum mechanical scattering results and quasiclassical trajectory results are available, only a small number of detailed comparisons of the two methods have been performed (see refs. 4 and 5 and references therein). The calculations presented here are, as a consequence, also used to extend the range of systems for which the reliability of QCT methods as compared to accurate quantal scattering methods is assessed.

The remainder of the paper is organised as follows. Sections II and III give details of the experiment and QCT and QM methodologies. Section II also gives the experimental results, and Section III gives theoretical results. The two kinds of theoretical results are discussed in Section IV, while the comparison between the experimental results and the theoretical predictions is examined in Section V. Concluding remarks are presented in Section VI. The appendix contains convergence checks for the QM calculations.

II. Experimental methods and results

The scattering experiments were carried out in a universal crossed molecular beam apparatus described in detail elsewhere.[2] Fig. 2 shows a schematic diagram of the set-up. Briefly, two well collimated supersonic beams of the reagents are crossed at 90° under single-collision conditions in a large scattering chamber with background pressure in the 10^{-7} mbar range. The angular and velocity distributions of the reaction products are recorded by a rotatable, triply differentially pumped, ultra-high-vacuum (10^{-11} mbar) electron impact ionization quadrupole mass spectrometer detector using time-of-flight (TOF) analysis. The two beam sources are usually doubly differentially pumped; to increase the product intensity for the experiments on $Cl + D_2$, however, the secondary D_2 beam source was brought close to the collision region with only one stage of differential pumping (we have verified in the case of the $Cl + H_2$ reaction that the product distributions are identical with or without using the second

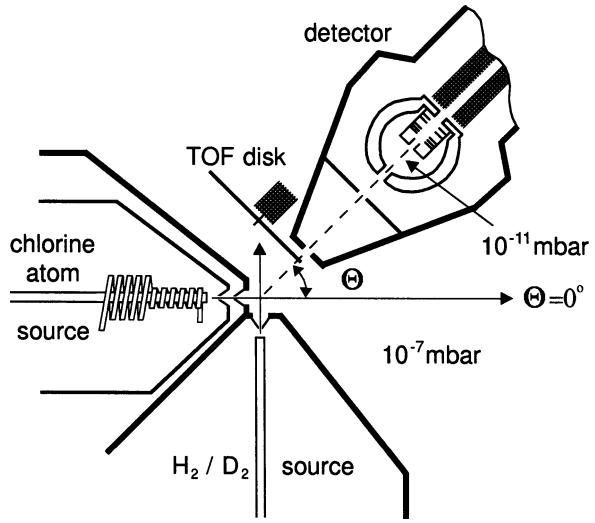

Fig. 2 Top view (cross sectional) of the crossed molecular beam apparatus, showing the doubly differentially pumped atomic chlorine beam source, the singly differentially pumped secondary molecular beam source (as in the Cl + D_2 experiment, see text), the triply differentially pumped electron-impact quadrupole mass spectrometer detector, and the time-of-flight chopper disk.

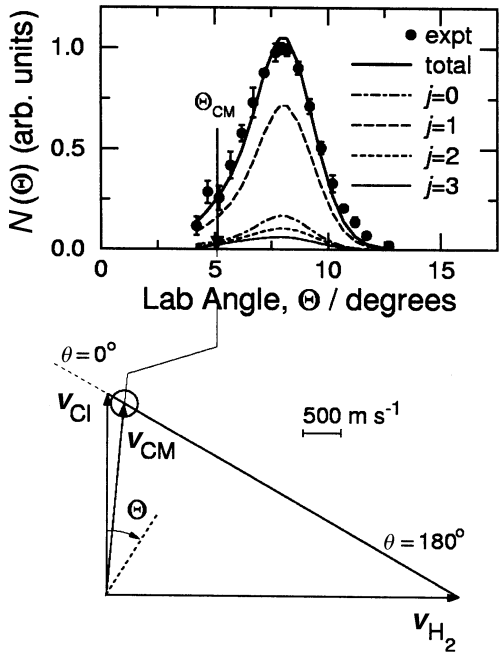

Fig. 3 HCl($v' = 0$) product laboratory angular distribution from the Cl + H_2($j = 0$, 1, 2, 3) reaction at $E_c = 5.85$ kcal mol^{-1} and corresponding canonical velocity vector ("Newton") diagram. The circle in the Newton diagram indicates the maximum speed that the HCl product can attain assuming that all the available energy is disposed into translation, *i.e.*, the speed of HCl($v' = 0$, $j' = 0$). The solid line represents the angular distribution obtained from the QM calculations on the G3 PES. The separate contributions from initial rotational levels of H_2 are also indicated.

differential stage). The H_2/D_2 beam source is pumped by 4200 and 2400 L s^{-1} diffusion pumps, while the Cl atom source features a 6000 L s^{-1} diffusion pump and a 2400 L s^{-1} differential diffusion pump; both beam sources are backed by 500 m^3 h^{-1} roots pumps.

The supersonic atomic chlorine beams were generated by a high-pressure radiofrequency (RF) discharge beam source, which has been used successfully in our laboratory for over a decade to generate intense supersonic beams of a variety of atomic and radical species.[2,25] The source is similar in design to that developed by Sibener *et al.*[26] to produce atomic oxygen beams. A high level of RF power was fed, through an LC circuit made to resonate around 14 MHz into a plasma contained in a quartz nozzle (diameter $\phi = 230$–250 μm) cooled by low electrical conductivity water. Due to the circuit design, the plasma is located behind the orifice of the nozzle, permitting a very high degree of molecular dissociation (up to 98%). Because of the high plasma temperature (up to 1900–2000 K) reached when a Cl_2–He mixture is used at high-pressure and high RF power, which in turn leads to a progressive nozzle enlargement over a relatively short (several hours) period of time, we operated by discharging gas mixtures that also included molecular oxygen (Cl_2–O_2–He mixtures). The plasma temperature is much lower in this case (~1200 K) and it is possible to operate at relatively high pressure (300–400 mbar) without losing beam stability.

For the Cl + H_2 experiment, we used a nominal RF power of 300 W in 300 mbar of a 2% Cl_2–2% O_2–96% He mixture, and the Cl beam peak velocity and speed ratio were 2650 m s^{-1} and 6.9, respectively, as measured from single-shot TOF analysis. The atomic chlorine beam was skimmed by a boron nitride skimmer ($\phi = 1$ mm) and further collimated by a rectangular slit (1.44 × 3.27 mm), which defines an angular divergence of 1.5°. The small angular divergence was critical in these experiments because the unfavourable kinematics confines the products within a small Newton sphere very close to the primary beam direction (see Fig. 3). The beam of H_2 was produced by supersonic expansion of neat H_2 at a stagnation pressure of 2.4 bar through a 100 μm stainless steel nozzle resistively heated at a nominal temperature of 858 K (corresponding to ~800 K) in order to increase the beam velocity. A skimmer ($\phi = 490$ μm) at a distance of 10 mm from the nozzle, followed by a 2.08 × 3.19 mm rectangular slit, defined an angular divergence of 2.9°. The peak velocity and speed ratio were 4400 m s^{-1} and 11.0, respectively. The canonical collision energy, E_c, of the experiment was 5.85 kcal mol^{-1}, with a collision energy spread of 1.40 kcal mol^{-1} FWHM. The rotational temperature of n-H_2(j) molecules in the beam was estimated to be ~300 K by extrapolating the consistent experimental determination of Pollard *et al.*;[27] the corresponding relative rotational populations are 0.13, 0.66, 0.12 and 0.09 for $j = 0$, 1, 2 and 3, respectively. We recall that the rotational energy content of the $j = 1$, 2 and 3 levels is 0.34, 1.02 and 2.04 kcal mol^{-1}, respectively (these energy contents are not negligible if we compare them to the energy barrier and the heat of reaction).

For the Cl + D_2 experiment, we used slightly different conditions for the atomic chlorine beam with a nominal RF power of 300 W in 250 mbar of a 1.25% Cl_2–2.5% O_2–96.25% He mixture; the Cl beam peak velocity and speed ratio were 2558 m s^{-1} and 6.9, respectively. In this experiment, because of smaller signal intensities and less unfavourable kinematics (*cf.* Figs. 3 and 4), we used a wider defining slit (2.08 × 3.19 mm) which enlarged the angular divergence to 2.3°. Moreover, to exploit the different kinematics we also used a beam obtained by discharging 120 mbar of the 2.5% Cl_2–He mixture without molecular oxygen at 140 W (a lower pressure and RF power were used for this gas mixture to limit the plasma temperature and hence to prevent nozzle enlargement); in this case, the peak velocity and speed ratio were 1930 m s^{-1} and 6.0, respectively.

The D_2 beam was produced by expanding neat D_2 at a stagnation pressure of 1.85 bar through a 100 μm stainless steel nozzle resistively heated to a nominal temperature of 703 K (corresponding to ~685 K). A skimmer ($\phi = 1.00$ mm) placed at 10 mm from the nozzle was the only defining element and gave an angular divergence of 5.7°. Peak velocity and speed ratio were 2892 m s^{-1} and 11.4. The canonical collision energy, E_c, of the experiment was 6.3 kcal mol^{-1} (with E_c spread of 1.4 kcal mol^{-1} FWHM). The rotational temperature of n-D_2(j) molecules in the beam was estimated to be

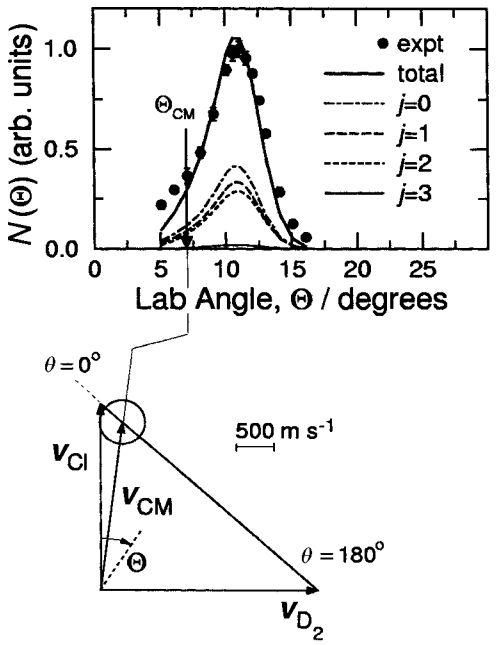

Fig. 4 DCl($v' = 0$) product laboratory angular distribution from the Cl + D_2($j = 0$, 1, 2, 3) reaction at $E_c = 6.3$ kcal mol^{-1} and corresponding Newton diagram. The circle in the Newton diagram indicates the maximum speed that the DCl product can attain assuming that all the available energy is disposed into translation, *i.e.*, the speed of DCl($v' = 0$, $j' = 0$). The solid line represents the angular distribution obtained from the QCT calculations on the G3 PES. The separate contributions from initial rotational levels of D_2 are also indicated.

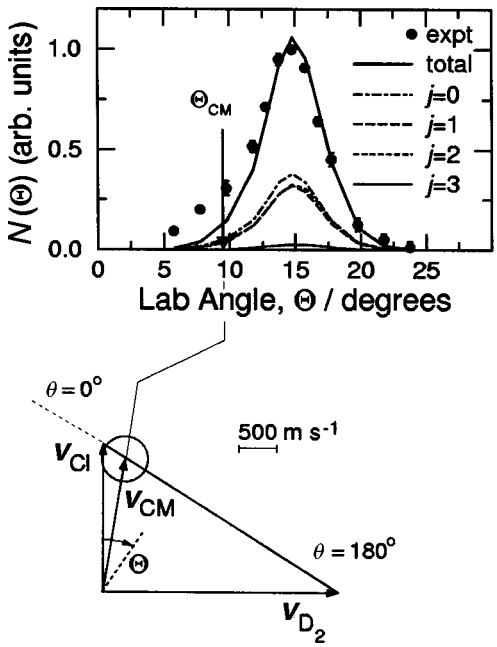

Fig. 5 DCl($v' = 0$) product laboratory angular distribution from the Cl + D_2($j = 0$, 1, 2, 3) reaction at $E_c = 6.4$ kcal mol^{-1} and corresponding Newton diagram. Solid and broken lines are as in Fig. 4. The different velocities of the reactant beams yield different kinematics than Fig. 4 even though the collision energy is similar to the experiment at $E_c = 6.3$ kcal mol^{-1}.

$\sim$260 K; the corresponding relative rotational populations are 0.21, 0.22, 0.39, 0.10 and 0.08 for $j = 0$, 1, 2, 3 and 4, respectively. The rotational energy content of the $j = 1$, 2, 3 and $j = 4$ levels is 0.17, 0.51, 1.03 and 1.71 kcal mol^{-1}, respectively. In the experiment where we used the 2.5% Cl_2–He mixture, the D_2 beam conditions were slightly different: the D_2 beam stagnation pressure was 2.2 bar, and the nominal temperature was kept at 873 K. Peak velocity and speed ratio were 3335 m s^{-1} and 10.6. The canonical collision energy, E_c, was 6.4 kcal mol^{-1}, which is very similar to the previous one, but the different kinematics helps to bring out some interesting features (see below, *cf.* Figs. 4 and 5).

It is well known that when an RF (or other electric) discharge is used to produce an atomic plasma, a manifold of electronic and fine structure levels of atomic species can be populated. Supersonic expansion is accompanied by a substantial relaxation to low-lying states. However, since unquenched excited states may affect the reaction dynamics, we characterised the atomic chlorine beams by Stern–Gerlach magnetic analysis.[28] The excited electronic states of chlorine atoms that involve orbital promotion are relatively high in energy and their presence (*i.e.*, their contribution to the observed product distributions) could be excluded on the basis of the observed signals and energetics; conversely, the $^2P_{1/2}$ spin–orbit excited state (located 2.52 kcal mol^{-1} above the ground state $^2P_{3/2}$) is formed in the plasma and is inefficiently quenched, as evidenced by magnetic analysis, which showed that about 15% of the Cl atoms are in the spin–orbit excited state. The presence of the excited state can affect the observed product distributions. In fact, the conventional opinion that spin–orbit excited states are hardly reactive has been challenged in recent studies of the F + H_2 and Cl + H_2 reactions,[11,29] where convincing evidence of spin–orbit-excited-state reactivity was given; unfortunately, the relative populations of $^2P_{1/2}$ and $^2P_{3/2}$ states have not been measured and so the relative reactivity of ground and excited spin–orbit states was only estimated.

The laboratory angular distributions, $N(\Theta)$ (*i.e.*, the number density as a function of the laboratory angle Θ), of the HCl and DCl products were obtained by taking at least five scans of 50 s counts at each angle. The nominal angular resolution of the detector for a point collision zone is 1°. The secondary target beam (H_2/D_2 beam) was modulated at 160 Hz with a tuning fork chopper for background subtraction. Even though ^{35}Cl is about three times more abundant than ^{37}Cl, we detected the scattered products at a mass to charge ratio (m/z) of 38 (H ^{37}Cl) and 39 (D ^{37}Cl), thus avoiding the detection of products at an m/z ratio between the intense peaks of the two atomic chlorine isotopes for Cl + H_2 and at the mass of non-reactively scattered ^{37}Cl in the case of ^{35}Cl + D_2. At the peak of the angular distributions the signal-to-noise ratio was about 40 and 80 for the Cl + H_2 and Cl + D_2 experiments, respectively.

Velocity distributions of the HCl and DCl products were obtained at selected laboratory angles using the cross correlation TOF technique with four 127-bit pseudorandom sequences. High-time resolution was achieved by spinning the TOF disk, located at the entrance of the detector, at 393.7 Hz, corresponding to a dwell time of 5 μs channel^{-1}. The flight length was 24.6 cm. Counting times varied from 30 to 60 min depending upon signal intensity.

The laboratory angular distributions from the Cl + H_2 reaction at $E_c = 5.85$ kcal mol^{-1} and from Cl + D_2 at the two similar collision energies, $E_c = 6.3$ and 6.4 kcal mol^{-1}, are shown in Figs. 3–5 together with the Newton diagrams corresponding to the most probable initial velocities. The error bars of the experimental distributions represent ± 1 standard deviation. Product TOF distributions at selected laboratory angles are shown in Figs. 6–8. The solid line in Figs. 3–8 represents the angular and TOF distributions obtained from QM (Cl + H_2) or QCT (Cl + D_2) calculations; the separate contributions from initial rotational levels of H_2 and D_2 are also indicated in the angular distribution figures (see Section IV.B). Figs. 3–5 also show that the HCl and DCl products are completely confined to the right of the center-of-mass (CM) position angle, that is, they are in the backward direction with respect to the Cl beam; the angular distributions are sharply peaked at an angle nearly tangent to the maximum Newton

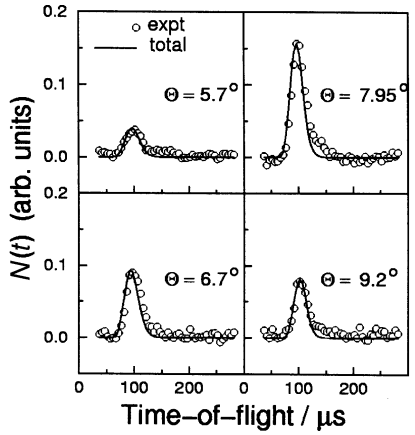

Fig. 6 HCl($v' = 0$) product time-of-flight distributions at selected laboratory angles from the Cl + H_2($j = 0$, 1, 2, 3) reaction at E_c = 5.85 kcal mol^{-1}. Solid lines are as in Fig. 3.

circle, which defines the angular range within which the products can be scattered on the basis of energy and linear momentum conservation. These features themselves suggest that the reaction mechanism is direct and of the rebound type and that a very large fraction of the available energy is released into relative translational motion of the products.

III. Theoretical methods

A. Quantum mechanical scattering calculations

The present calculations were performed using the outgoing wave variational principle[30–35] (OWVP); details of this method and its computational implementation have been presented elsewhere.[30,33,35–38] The calculations decouple into blocks depending on the total angular momentum J, the parity P and the homonuclear interchange symmetry S, and each of these blocks may be solved separately. Results may be

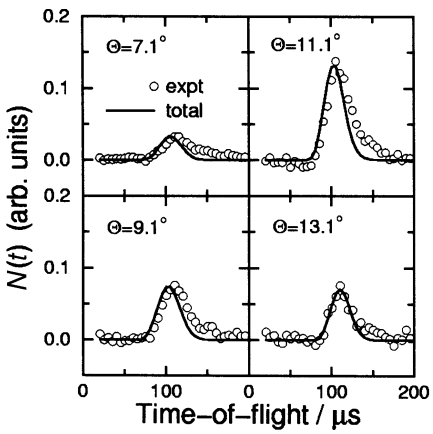

Fig. 7 DCl($v' = 0$) product time-of-flight distributions at selected laboratory angles from the Cl + D_2($j = 0$, 1, 2, 3) reaction at E_c = 6.3 kcal mol^{-1}. Solid lines are as in Fig. 4.

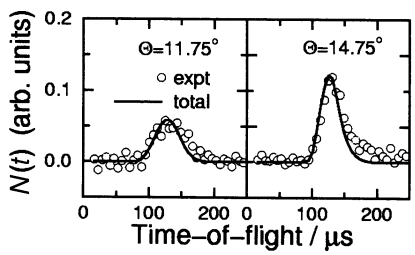

Fig. 8 DCl($v' = 0$) product time-of-flight distributions at selected laboratory angles from the Cl + D_2($j = 0$, 1, 2, 3) reaction at E_c = 6.4 kcal mol^{-1}. Solid lines are as in Fig. 5.

obtained for initial states with rotational quantum number $j = 0$ by solving only one of the four PS blocks for each $J > 0$ (or two PS blocks for $J = 0$). In the present work, we study the effects of rotational excitation on the differential cross sections, and we solve all four PS combinations to treat the range of initial states selected; relatively few studies[24,39–43] have been presented for more than one initial rotational state, in part, because of this increased computational expense. Some work involved in the formation of the matrix elements of the variational functional for the two different S blocks of a given J and P is the same for both blocks; the present calculations exploit this by forming the matrix elements for these two blocks simultaneously.

The numerical and basis set parameters are optimised separately for each system and energy studied; however, certain details are common to all the present calculations. In particular, we use body-frame basis functions[37,44,45] and complex boundary conditions; by judicious use of boundary condition transformations and partitioned matrix techniques[46,47] the actual formation of the matrix elements, as well as the bulk of the work in the solution of the resulting linear system, is accomplished in real arithmetic and at a computational cost that is only slightly greater than would be the case for real boundary conditions.

A body-frame basis set truncation method[37,40,48,49] is employed based on the magnitude, Ω^{max}, of the projection of the total angular momentum on the atom-to-diatom axis in a given arrangement. All open channels with $\Omega > \Omega^{max}$ are limited to one translational basis function and closed channels with $\Omega > \Omega^{max}$ are not included. In general the value of Ω^{max} is taken to be a function of the channel quantum numbers.

All radial translational functions in open channels are rotationally coupled half-integrated Green's functions[38] (HIGFs) and we used distributed Gaussian translational functions in all closed channels. The coupling scheme[30,33,37] used to define the distortion potential coupled all channels with $j \leqslant j_\alpha^d(v)$ in a given arrangement and vibrational manifold and employs single-state coupling (*i.e.*, all channels with the same v, j and α) for channels with $j > j_\alpha^d(v)$. In tables, when we write $j_\alpha^d(v) = \infty$ this indicates that all $j \leqslant j_{max}(\alpha, v)$ (the maximum rotational level in the basis set for a given α and v) are coupled for a given arrangement.

For all production runs, calculation of matrix elements of the variational functional involving both of the identical heteronuclear arrangements was neglected[30,33] (*i.e.*, replaced by zero); this significantly reduces the cost of the matrix element evaluation while producing negligible error in the transition probabilities involving the homonuclear arrangement (the high accuracy of this approximation was demonstrated in convergence checks which showed the error to be small in comparison to the basis set truncation error, which is itself small for these calculations). This approximation is indicated in our parameter set notation by $N_{23}^{QA} = 0$.

All cross section calculations were carefully converged with respect to basis sets and numerical parameters. These convergence checks and a description of the basis set parameters are presented in the Tables A-I, A-II, A-III, A-IV and A-V of the Appendix.‡

All results are summed over the two identical heteronuclear arrangements.

For a given J and total energy E, we define the state-to-state distinguishable-atom reaction probabilities by

$$P_{vjv'j'}^{J} = \frac{1}{2\ \min(J, j) + 1} \sum_{P} \sum_{\alpha' \neq 1} \sum_{l} \sum_{l'} |S_{\alpha' v' j' l' 1 v j l}^{JP}|^2 \qquad (1)$$

where $S_{\alpha' v' j' l' 1 v j l}^{JP}$ is a scattering matrix element, α is an arrangement label ($\alpha = 1$ for Cl + H_2, $\alpha' = 2$ or 3 for the two identi-

‡ Available as electronic supplementary information. See http://www.rsc.org/suppdata/cp/a9/a908829f

cal HCl + H arrangements), l is the orbital angular momentum quantum number associated with relative translational motion, and primes denote final values.

The state-to-state partial integral cross sections are defined by

$$\sigma^{J}_{vjv'j'} = \frac{\pi}{k^2_{vj}} \frac{2J+1}{2j+1} \sum_{P} \sum_{\alpha' \neq 1} \sum_{l} \sum_{l'} |S^{JP}_{\alpha' v' j' l' 1 v j l}|^2, \quad (2)$$

where k_{vj} is the initial state wavenumber. The integral cross sections can be defined by

$$\sigma_{vjv'j'} = \sum_{J=0}^{J_{max}} \sigma^{J}_{vjv'j'} \quad (3)$$

where J_{max} is the largest total angular momentum included in the calculation; it will also be convenient to define the cross sections summed over the final rotational states, *i.e.*,

$$\sigma_{vjv'} = \sum_{j'} \sigma_{vjv'j'}. \quad (4)$$

The state-to-state reactive opacity function, *i.e.*, the state-to-state reaction probability as a function of l, is defined as

$$P_{vjv'j'}(l) = \frac{1}{(2j+1)(2l+1)} \times \sum_{P} \sum_{\alpha' \neq 1} \sum_{J} \sum_{l'} (2J+1) |S^{JP}_{\alpha' v' j' l' 1 v j l}|^2; \quad (5)$$

in terms of which the state-to-state cross sections are given by

$$\sigma_{vjv'j'} = \frac{\pi}{k^2_{vj}} \sum_{l} (2l+1) P_{vjv'j'}(l). \quad (6)$$

Differential cross sections were calculated using the formula

$$\frac{d\sigma_{\alpha v j \alpha' v' j'}}{d\Omega} = \frac{\pi}{(2j+1)k^2_{vj}} \sum_{m_j=-j}^{j} \sum_{m_{j'}=-j'}^{j'} \times \left| \sum_{J} \sum_{M=-J}^{J} \sum_{l=|J-j|}^{J+j} \sum_{l'=|J-j'|}^{J+j'} \sum_{\mu=-l'}^{l'} (2l+1)^{1/2} \times (l_j 0 m_j | l_j J M)(l'_j \mu m'_j | l'_j J M)(\delta_{\alpha'\alpha} \delta_{v'v} \delta_{j'j} \delta_{l'l} - S_{v'j'l'vjl}) Y_{l'\mu}(\pi - \theta, \phi) \right|^2 \quad (7)$$

where θ and ϕ are the final angular coordinates of the scattered particle in the center-of-mass frame, and $\Omega \equiv (\theta, \phi)$.

The differential cross section summed over the final rotational quantum number is defined as

$$\frac{d\sigma_{vjv'}}{d\Omega} = \sum_{j'} \frac{d\sigma_{\alpha v j \alpha' v' j'}}{d\Omega} \quad (8)$$

where the arrangement subscript α has been dropped for clarity (it is understood for the present application that α is the label of the reactant arrangement, and α' is the label of the product arrangement).

Table 1 details the QM scattering calculations performed for this study for comparison to the Cl + H_2 experiment at $E_c = 5.85$ kcal mol^{-1} and the Cl + D_2 experiment at $E_c = 6.3$ kcal mol^{-1}. Calculations at other energies were also performed (see below). The table reports values for the total energy, collision energy, maximum value of the total angular momentum, initial and final values of the vibration and rotation quantum numbers (j' is given as a range), and the range of orbital angular momentum values.

In brief, calculations were performed at the fixed collision energy $E_c = 5.85$ kcal mol^{-1} for Cl + H_2 ($v = 0$, $j = 0$, 1 and 2) and at $E_c = 6.20$ kcal mol^{-1}, 6.03 kcal mol^{-1} and 5.68 kcal mol^{-1} for Cl + D_2 ($v = 0$, $j = 0$, 1 and 2), respectively. For Cl + D_2 this corresponds to a total energy E of 10.60 kcal mol^{-1}, and it means that calculations were performed at one constant total energy. Additionally, calculations were performed for Cl + H_2($v = 0$, $j = 0$) at $E_c = 4.0$, 4.9, 6.2 and 6.9 kcal mol^{-1}, and for Cl + D_2($v = 0$, $j = 0$) at $E_c = 9.10$ kcal mol^{-1} and $E_c = 10.27$ kcal mol^{-1}.

B. Quasiclassical trajectory calculations

The general method for the quasiclassical trajectory calculations has been described in detail previously (see refs. 50 and 51 and references therein), and only the details relevant to the present work will be given here. We note, for non-specialists, that the "quasi" in "quasiclassical" refers to selecting the initial conditions of the trajectories with quantized vibrational and rotational energies. After that, motion is calculated by Hamilton's classical mechanical equations and, after the collision, the unquantized classical variables are used to estimate quantized final states by the "histogram" or "binning" method.

Calculations were first performed for the Cl + H_2($v = 0$, $j = 0$–3) reaction on the G3 PES at the fixed collision energy $E_c = 5.85$ kcal mol^{-1}. Batches of 50000 trajectories were run for each initial j. Additionally, calculations were performed for Cl + H_2($v = 0$, $j = 0$) at $E_c = 4.0$, 4.9, 6.2 and 6.9 kcal mol^{-1}. For the Cl + D_2($v = 0$, j) reaction, batches of 50000 trajectories were run for $j = 0$ and $E_c = 6.20$ kcal mol^{-1}, $j = 1$ and $E_c = 6.03$ kcal mol^{-1} and $j = 2$ and $E_c = 5.68$ kcal mol^{-1} to compare with the QM calculations. In addition, batches of 50 000 trajectories were run for the Cl + D_2 reaction at $j = 0$, 1 and $j = 2$ and $E_c = 6.4$ kcal mol^{-1} in order to simulate the experimental results. Finally, batches of 50000 trajectories were run for Cl + D_2($v = 0$, $j = 0$) at $E_c = 9.10$ and 10.27 kcal mol^{-1} for comparison with QM results. The integration step size in the trajectories was chosen to be 5×10^{-17} s. This guarantees conservation of the total energy to better than 1 part in 10^5 and conservation of total angular momentum to better than 1 part in 10^7. As usual, the rovibrational energies of the H_2(D_2) reagent and those of the HCl and DCl products are calculated by semiclassical quantization of the action using the potential given by the asymptotic diatom limits of the G3 PES. These rovibrational energies are fitted to Dunham expansions containing 20 terms (fourth power in $v + \frac{1}{2}$ and third power in $j(j+1)$). The assignment of product quantum numbers (v', j') is carried out by equating the classical rotational angular momentum of the product molecule to $[j'(j'+1)]^{1/2}(h/2\pi)$. With the (real) j' value so obtained, the vibrational quantum number v' is found by equating the internal energy of the outgoing molecule to the corresponding Dunham expansions. The values of v' and j' found in this way are then rounded to the nearest integer.

The state-resolved differential cross sections were calculated

Table 1 Summary of quantal calculations performed in this study; the total energy (E) and collision energy (E_c) are in kcal mol^{-1}

System	E	J_{max}	E_c	v	j	v'	j'	l
Cl + H_2	12.04	30	5.85	0	0	0	0–12	0–30
	12.38	30	5.85	0	1	0	0–12	0–31
	13.06	30	5.85	0	2	0	0–12	0–32
Cl + D_2	10.60	34	6.20	0	0	0	0–16	0–34
	10.60	34	6.03	0	1	0	0–16	0–35
	10.60	34	5.68	0	2	0	0–16	0–36

by expansion in Legendre polynomials (see refs. 50–53). The Smirnov–Kolmorogov test comparing the cumulative probability distributions was used as the criterion for truncation of the series. Significance levels higher than 98% could be achieved using 6–10 Legendre moments, ensuring very good convergence such that the inclusion of more terms does not produce any significant change.

As in previous work,[17,54,55] the collision energy dependence of the reaction cross section, $\sigma_R(E_c)$, was determined by running batches of trajectories where the collision energy is sampled randomly within the interval $[E_1, E_2]$. The E_1 energy value is chosen so that the collisional threshold, E_0, is larger than E_1. Once the value of the collision energy is randomly (uniformly) sampled within $\Delta E = E_2 - E_1$, the impact parameter b is obtained for every trajectory as

$$b = \beta^{1/2} b_{max}(E_c) \tag{9}$$

where β is a random number in the [0,1] interval, and the maximum impact parameter, b_{max}, at a given collision energy, E_c, is given by

$$b_{max}(E_c) = D\left(1 - \frac{E_D}{E_c}\right)^{1/2} \tag{10}$$

The values of the parameters D and E_D (where $E_D < E_1 < E_0$) are previously determined by fitting the values of the maximum impact parameters, found at several selected collision energies, E_c, to the line-of-the-centers expression of eqn. (10). The resulting $b_{max}(E_c)$ are such that, for the selected E_c, there are no reactive trajectories for impact parameters larger than b_{max}. With this kind of energy-dependent sampling of the impact parameter, each trajectory is weighted by $w_i = b_{max}^2/D^2$. Batches of 50000 trajectories for every (v, j) rovibrational state of H_2 and D_2 have been run in the energy range from threshold up to 18 kcal mol^{-1} on the G3 PES. The excitation functions, $\sigma_R(E_c)$, were subsequently calculated by expansion in Legendre polynomials (see refs. 17, 54 and 55) using the reduced variable,

$$r = \frac{2E_c - E_2 - E_1}{\Delta E} \tag{11}$$

where $\Delta E = E_2 - E_1$. The expression for $\sigma_R(E_c)$, truncated after the Mth order Legendre polynomial, is given by

$$\sigma_R(E_c) = \frac{2R}{\Delta E}\left[\frac{1}{2} + \sum_{n=1}^{M} b_n P_n(r)\right] \tag{12}$$

where R is the Monte Carlo estimate of the integral

$$R = \langle \sigma_R(E_c) \rangle \Delta E = \int_{E_1}^{E_2} \sigma_R(E_c) dE_c \approx \pi D^2 \Delta E \frac{S_{N_R}}{N} \tag{13}$$

N is the total (reactive and non-reactive) number of trajectories, and the sum, S_{N_R}, of the weights (w_i) of the reactive trajectories is given by

$$S_{N_R} = \sum_{i=1}^{N_R} w_i \tag{14}$$

The coefficients, b_n, of the Legendre expansion of eqn. (12) are calculated as the Monte Carlo average of Legendre moments

$$b_n = \frac{2n+1}{2} \frac{1}{S_{N_R}} \sum_{i=1}^{N_R} w_i P_n(x_i) = \frac{2n+1}{2} \langle P_n \rangle \tag{15}$$

The corresponding expressions to calculate the standard errors in the coefficients and the reaction cross sections can be found in refs. 54 and 55.

The method to calculate the collision energy dependence of the DCS is similar to that described above but uses a double expansion in Legendre polynomials with arguments r and $\cos\theta$:

$$\frac{d\sigma_R}{d\omega}(E_c) = \frac{2R}{2\pi\Delta E}\left[\frac{1}{4} + \frac{1}{2}\sum_{m=1}^{M} a_m P_m(\cos\theta) + \frac{1}{2}\sum_{n=1}^{N} b_n P_n(r) + \sum_{m=1}^{M}\sum_{n=1}^{N} \alpha_{mn} P_n(\cos\theta) P_n(r)\right] \tag{16}$$

The value of α_{mn} is the Monte Carlo average of $(2m + 1)P_m(\cos\theta)(2n + 1)P_n(\cos\theta)/4$ over the total number of trajectories. See ref. 5 for more details.

The energy evolution of the reaction probability at total angular momentum $J = 0$, $P^{J=0}(E)$, for the $Cl + H_2(v = 0, j = 0)$ reaction has been calculated by running a batch of 50000 trajectories with zero impact parameter and using the method of moments expansion in Legendre polynomials as described in ref. 51.

C. Electronic degeneracy

None of the theoretical cross sections (either quasiclassical or quantal) have been multiplied by a factor to take account of the electronic degeneracy; thus they correspond to cross sections for collisions that occur on the ground electronic surface of the three-body system. To convert them to experimentally observable cross sections for the $Cl(^2P_{3/2})$ state without state selection on the M_J quantum number of the atom, they should all be multiplied by 0.5, which is the ratio of the electronic degeneracy (2) of the three-body ground state to the electronic degeneracy (4) of the infinitely separated ground state reactants.[56]

IV. Theoretical results

A. Reaction probabilities as a function of total energy

Fig. 9 depicts the comparison between the QM and QCT total and vibrationally state-resolved reaction probabilities as functions of the total energy for the ground-state reaction of H_2 with total angular momentum J equal to 0 on the G3 PES. The two sets of theoretical results agree qualitatively, with the general shape of the quantal $P^{J=0}(E)$ being well reproduced by the classical calculations. The QM $P^{J=0}(E)$ curve, however, shows more structure. Except for the lower total energies, the QM reaction probabilities are larger than the classical ones, although for $E > 18$ kcal mol^{-1}, the results are very similar.

The thresholds for the appearance of HCl in $v' = 0$ and $v' = 1$ deserve special attention. The threshold for HCl($v' = 0$)

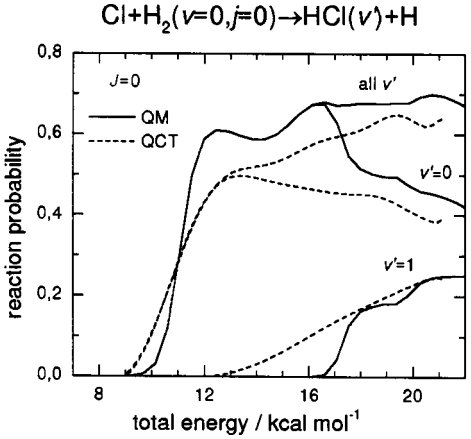

Fig. 9 Total and vibrationally state-resolved QM (——) and QCT (– – –) reaction probabilities as a function of total energy for the Cl + $H_2(v = 0, j = 0)$ reaction calculated at total angular momentum $J = 0$ on the G3 PES.

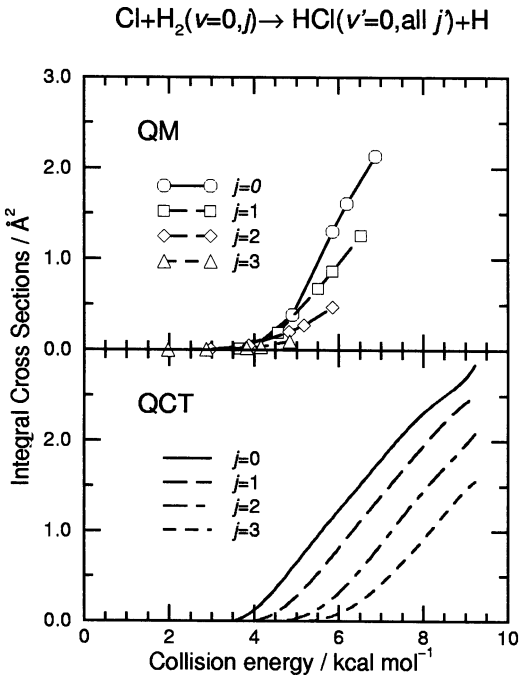

Fig. 10 Integral cross sections as functions of collision energy, *i.e.*, excitation functions, for the Cl + H_2(j = 0, 1, 2, 3) reaction. (Top) QM calculations. (Bottom) QCT calculations. All the calculations have been carried out on the G3 PES.

is somewhat above the classical barrier of the G3 PES (7.88 kcal mol^{-1}). This means that not all the vibrational energy of H_2(v = 0, j = 0) is employed to surmount the barrier, even in classical mechanics. This is consistent with a myriad of previous quasiclassical studies; for example, similar behaviour has been found for the D + H_2 reaction,[57] where roughly half of the v = 0 vibrational quantum was used to overcome the classical barrier. Below the classical threshold, tunnelling is the only possible mechanism for HCl production. Interestingly, however, the quantal reactivity is found to be smaller than the classical one at E < 10.38 kcal mol^{-1}, and therefore, tunnelling does not compensate the effect of the zero-point energy of the transition state; as a consequence, the effective threshold is underestimated in the QCT calculation. For the production of HCl(v' = 1), the smaller threshold obtained in the QCT calculations as compared to the QM ones has a very different origin; namely, the quasiclassical binning of final states which is made by rounding the continuous classical v' value to the allowed discrete value (nearest integer). This compounds the error of not quantizing the dynamical bottleneck, and the threshold error is larger for v' = 1 than for v' = 0. The purely thermodynamical threshold for HCl(v' = 1) is 15.45 kcal mol^{-1}, only slightly smaller than the energy where the QM probability for v' = 1 production becomes significant in Fig. 9. If only those trajectories with vibrational energy above v' = 1 were allocated into v' = 1 state, the classical threshold would be of course very near the QM one. However, if this naive criterion were used for energies above the v' = 1 threshold, the resulting $P^{J=0}_{v'=1}(E)$ would be much smaller than the quantal one. This is a limitation of the QCT approach itself, and no simple solution is available.

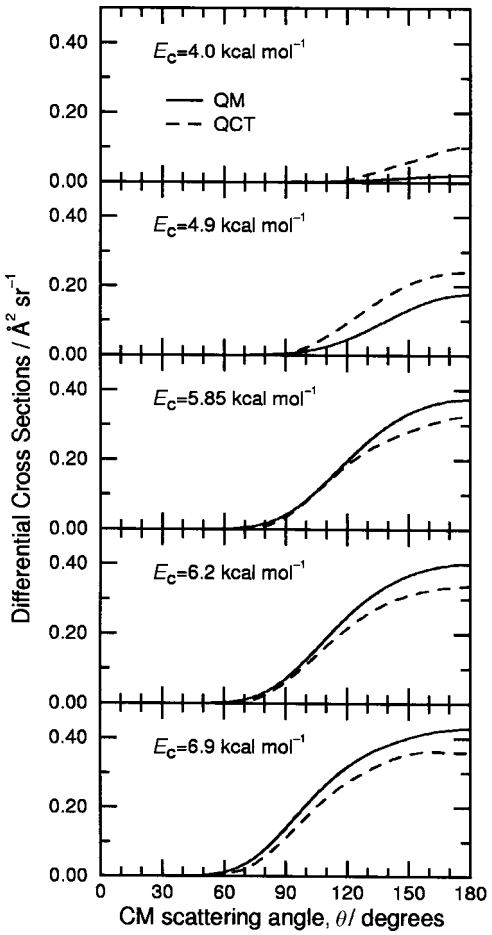

Fig. 11 QM (——) and QCT (– – –) differential cross sections for the Cl + H_2(v = 0, j = 0) → HCl(v' = 0) + H reaction calculated on the G3 PES at five collision energies ranging from 4.0 to 6.9 kcal mol^{-1}.

B. Integral and differential cross sections

The QM and QCT collision energy dependence of the integral cross sections, *i.e.* the excitation functions $\sigma_R(E_c)$, calculated for the Cl + H_2(v = 0, j = 0–3) reaction on the G3 PES are shown in Fig. 10. In both cases, reactivity decreases as the reagent rotational quantum number increases. The main difference between the QCT and QM excitation functions is that whereas the classical translational energy threshold increases substantially with initial j, the QM one remains practically unchanged, in spite of the negative effect of rotational excitation on the reaction cross section at collision energies immediately above the threshold. This same behaviour has been observed also in QCT studies on the D + H_2 reaction.[54] The negative influence of reagent rotation on reactivity has been extensively described for different reactions and various explanations in terms of dynamical models have been advanced; reviews of the early work are available.[58] The subject has been discussed more recently by Aoiz *et al.*[17,54,55] and Song and Gislason[59] where strongly collinear surfaces were used; the general idea that has been proposed of how rotation affects the classical results is that the forces outside the barrier tend to steer the reactants into the cone of acceptance in the absence of rotation. Reagent rotation would hinder this steering, leading to a decline of the integral cross sections with j for the first rotational quantum, thus diminishing the possible orienting effect of the PES. These effects are augmented if, as in the case of the G3 PES, the PES is collinearly dominated. The fact that in the QM case, an increase of the reaction threshold with increasing rotational excitation is not observed can be explained by an enhancement of tunnelling as j increases,[54] but a more likely explanation involves the tendency of successive rotational states to couple to the same quantized transition state.[19,60]

There is experimental evidence[10] for the Cl + H_2 reaction that the effect of reagent rotation should be positive (not negative as in the present QM and QCT calculations on the G3 PES). Lee *et al.*[10] have, in fact, measured state-specific excitation functions for the Cl + *para*-H_2 and Cl + *normal*-H_2 reactions, and from them they have deduced excitation functions for the reactions with j = 0 and j = 1. Both excitation functions have the same relative translational energy threshold to

reaction, but as collision energy increases the cross sections for the reaction with $j = 1$ become larger than for $j = 0$. The authors attribute the discrepancies between dynamical calculations on the G3 PES and their experimental data to deficiencies of the G3 PES.

Fig. 11 shows the QM and QCT DCSs for the Cl + $H_2(v = 0, j = 0)$ reaction at collision energies ranging from 4.0 kcal mol^{-1} to 6.9 kcal mol^{-1}. Both theoretical approaches predict backward DCSs that include larger sideways contributions as collision energy increases. The QM and QCT DCSs agree reasonably well in general shape, but, whereas the total QCT integral cross section is larger than the QM one at low collision energies, at $E_c \geqslant 5.85$ kcal mol^{-1} the behaviour becomes the opposite. As in the case of the $J = 0$ reaction probabilities discussed above, the classical threshold for initial $j = 0$ lies below the QM one. Therefore, also in the case of summing over all angular momenta, the error in QCT due to neglecting tunnelling does not cancel the error due to neglecting the zero-point energy at the transition state.

The HCl($v' = 0$) product rotational distributions are shown in Fig. 12. Interestingly, for $E_c \geqslant 5.85$ kcal mol^{-1} the QM and QCT distributions peak at the same j' values. However, at collision energies smaller than 5.85 kcal mol^{-1}, the QCT distributions are significantly cooler than the QM ones. This may be surprising since one of the shortcomings of the QCT approach, which is related to the method of assigning quantum numbers to the product molecules, is that it often yields hotter rotational distributions than the QM method. Overall, the best agreement between QM and QCT DCSs and product rotational distributions for Cl + $H_2(v = 0, j = 0)$ is obtained at $E_c = 5.85$ kcal mol^{-1}.

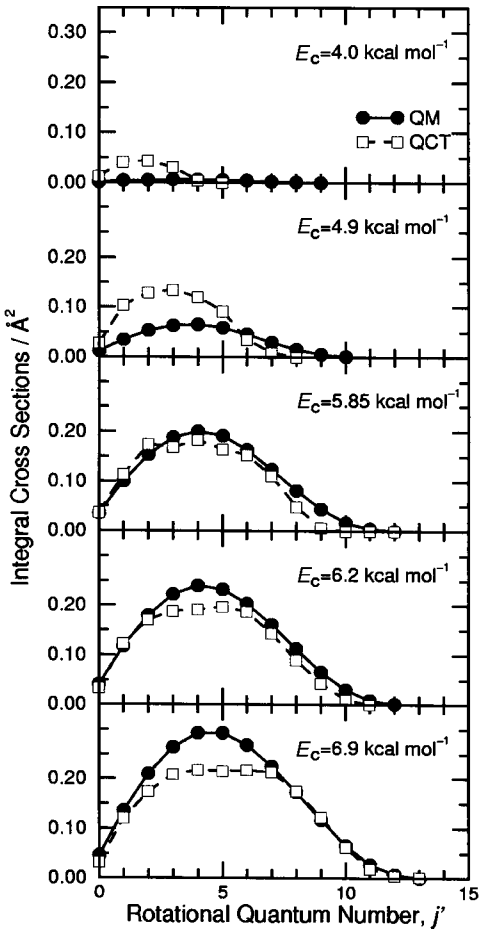

Fig. 12 QM (–●–) and QCT (–□–) integral cross sections as a function of the final rotational state j' of the HCl($v' = 0$) product from the Cl + $H_2(v = 0, j = 0)$ reaction calculated on the G3 PES at five collision energies ranging from 4.0 to 6.9 kcal mol^{-1}.

The QM and QCT total DCSs for the Cl + $H_2(v = 0, j = 0, 1, 2, 3)$ reactions calculated at $E_c = 5.85$ kcal mol^{-1} are depicted in Fig. 13, and the corresponding product rotational distributions are shown in Fig. 14. The agreement between QM and QCT DCSs and j' distributions at this collision energy is good for initial $j = 0$ and $j = 1$ and becomes somewhat worse at $j = 2$ (for $j = 3$ the QM data are not presented). The negative effect of initial rotation on reactivity is clearly seen in the smaller DCS values and integral cross sections obtained as initial j increases. The QM DCSs are more sideways than the QCT ones for $j = 1$ and, specially, for $j = 2$, where the QM reactive scattering reaches angles up to $\theta = 60°$, in contrast with the $\theta = 100°$ in the QCT case. The

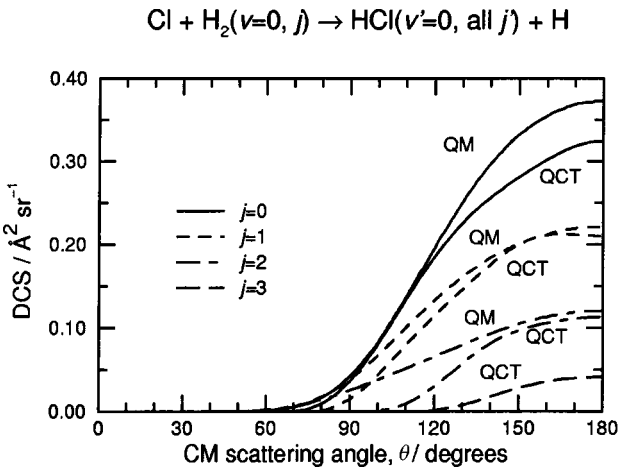

Fig. 13 QM and QCT differential cross sections for the Cl + $H_2(v = 0, j = 0) \rightarrow$ HCl($v' = 0$) + H reactions calculated on the G3 PES at $E_c = 5.85$ kcal mol^{-1}.

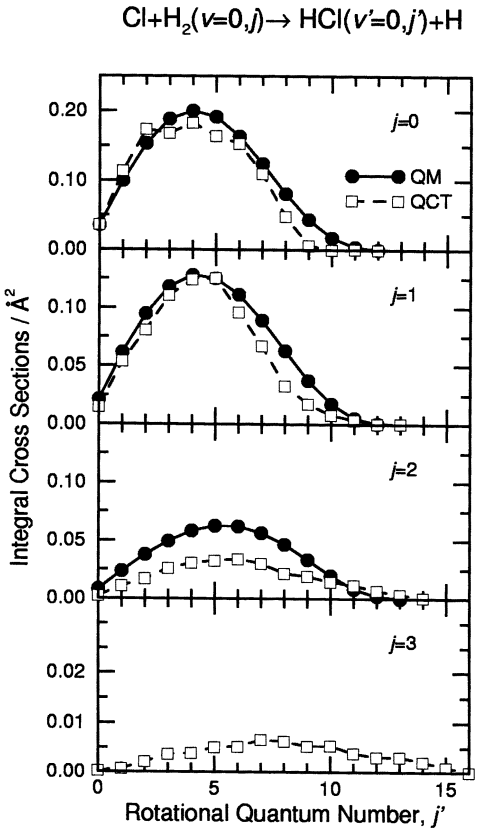

Fig. 14 QM (–●–) and QCT (–□–) integral cross sections as a function of the final rotational state j' of the HCl($v' = 0$) product from the Cl + $H_2(v = 0, j = 0, 1, 2, 3)$ reaction calculated on the G3 PES at $E_c = 5.85$ kcal mol^{-1}.

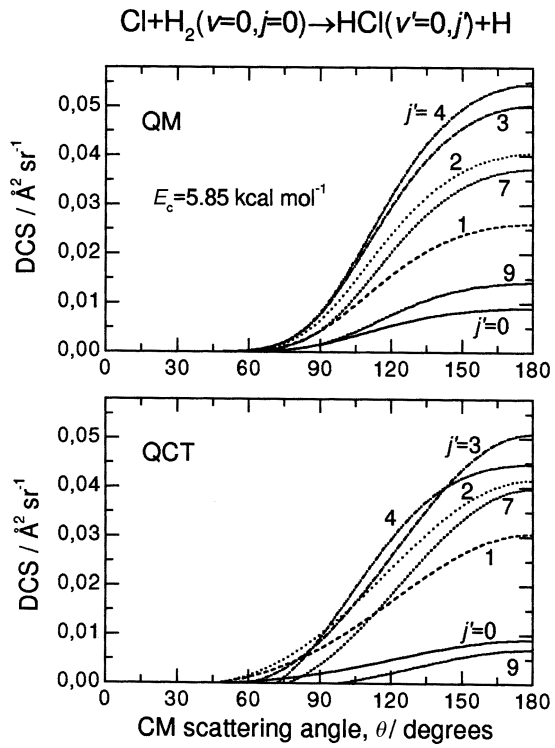

Fig. 15 Selected QM (top) and QCT (bottom) rovibrationally state-resolved differential cross sections for the Cl + H_2($v = 0$, $j = 0$) reaction calculated on the G3 PES at $E_c = 5.85$ kcal mol^{-1}.

QCT product rotational distributions peak at the same j' values as the QM ones.

Fig. 15 depicts selected QM and QCT rovibrationally state-resolved DCSs for the Cl + H_2($v = 0$, $j = 0$) → HCl($v' = 0$, j') + H reaction at $E_c = 5.85$ kcal mol^{-1}. Good agreement is found for most of the j' states. However, to construct the QCT DCSs, only 3–4 moments of the Legendre expansion were used, although the Smirnov–Kolmogorov statistical test based on the analysis of the cumulative probabilities (see Section III.B) indicated that more moments were needed to obtain significance levels higher than 0.9. This implies that the first few moments of the QM and QCT expansions are very similar. Nevertheless, whereas in the QM case higher moments become negligible, in the QCT case the number of moments significantly different than zero are larger (about 6–8). If all the moments required by the statistical analysis to obtain significance levels larger than 0.9 are included, the DCSs would be more structured, deviating from the QM ones. The same behaviour has been observed previously for the H + D_2 reaction at low collision energies,[55,61,62] and it may be a symptom of the difficulty of deciding which moments are meaningful, not a true difference of classical and quantum mechanics. In

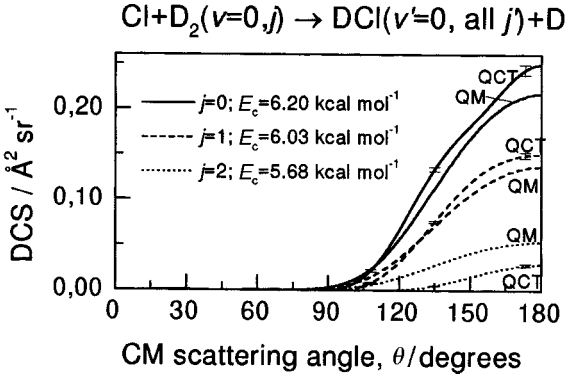

Fig. 16 QM and QCT differential cross sections for the Cl + D_2($v = 0$, $j = 0$, 1, 2) → DCl($v' = 0$) + D reaction at the collision energies $E_c = 6.20$, 6.03 and 5.68 kcal mol^{-1}.

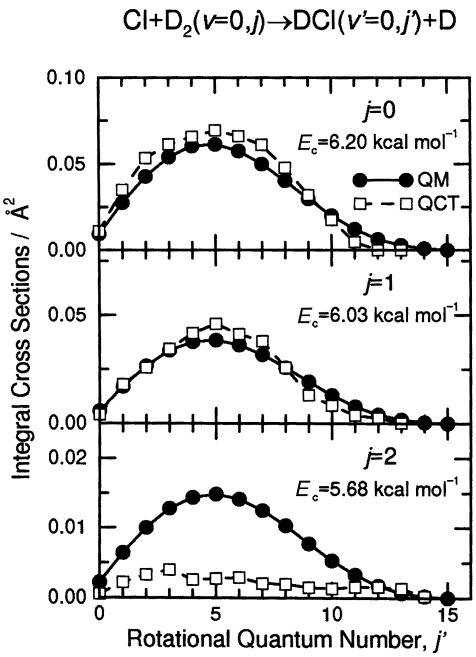

Fig. 17 QM (–●–) and QCT (–□–) integral cross sections as a function of the final rotational state j' of the DCl($v' = 0$) product for the Cl + D_2($v = 0, j = 0$, 1, 2, 3) reaction calculated on the G3 PES at the collision energies $E_c = 6.20$, 6.03 and 5.68 kcal mol^{-1}.

contrast, for the QM and QCT vibrationally state-resolved DCSs, the number of moments significantly different than zero were the same.

Figs. 16 and 17 depict the comparison of the QM and QCT DCSs and product rotational distributions for the Cl + D_2($v = 0$, $j = 0$, 1, 2) case at collision energies of 6.20–5.68 kcal mol^{-1} (fixed total energy of 10.60 kcal mol^{-1}). The agreement between the results obtained from the two theoretical approaches is similar to what was observed for the Cl + H_2 case; in particular, the shapes of the DCSs are very similar (backward scattering), but the QCT integral cross

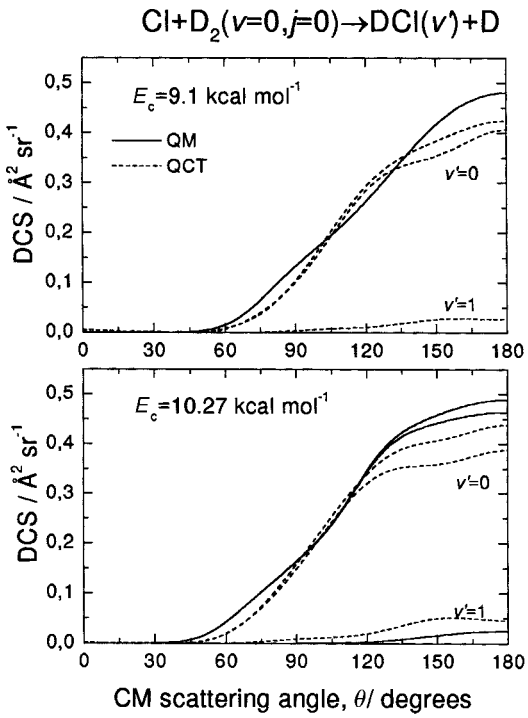

Fig. 18 QM (——) and QCT (- - - - -) total and vibrationally state-resolved differential cross sections for the DCl($v' = 0$) product of the Cl + D_2($v = 0, j = 0$) reaction obtained from calculations at $E_c = 9.1$ kcal mol^{-1} (top) and 10.27 kcal mol^{-1} (bottom).

section is larger for $j = 0$, 1 and substantially smaller for $j = 2$ as compared with the QM results. The good agreement extends to higher collision energies as shown in Fig. 18, where the QM and QCT total and v' state-resolved DCSs for the $Cl + D_2(v = 0,\ j = 0)$ reaction calculated at $E_c = 9.1$ kcal mol^{-1} and 10.27 kcal mol^{-1} are shown. At $E_c = 9.1$ kcal mol^{-1} the $v' = 1$ product channel is not energetically accessible. However, due to the quasiclassical assignment of final vibrational states (see Section III.B), all the trajectories labelled $v' = 1$ have a vibrational energy less than that corresponding to that state, *i.e.*, classical analogs of the vibrational numbers between 0.5 and 1.0, and, consequently, reactivity into $v' = 1$ is found in the QCT case.

V. Comparison between experimental results and theoretical predictions

The QM and QCT differential cross sections are calculated in the center-of-mass (CM) coordinate system, and to compare them to experiment we must convert them to the laboratory (LAB) system of coordinates. The relation between LAB and CM fluxes is given by:

$$I_{LAB}(\Theta, v) = I_{CM}(\theta, u)v^2/u^2 \tag{17}$$

(where Θ and v are LAB angle and final speed of products, respectively, and θ and u are the corresponding CM quantities), *i.e.*, the scattering intensity observed in the laboratory is distorted by the transformation Jacobian v^2/u^2 from that in the CM system. However, since the electron impact ionisation mass spectrometric detector measures the number density of products, $N_{LAB}(\Theta)$, not their flux, the actual relation that we require between the LAB observable and the CM flux is given by:

$$N_{LAB}(\Theta, v) = I_{CM}(\theta, u)v/u^2. \tag{18}$$

Due to the finite experimental resolution (*i.e.*, finite angular and velocity spread of the reactant beams and angular resolution of the detector) the LAB-CM transformation is not single-valued and, therefore, analysis of the laboratory data has been carried out by forward convolution over the experimental conditions of the theoretically derived CM functions.

The shape of the LAB angular and TOF distributions of Figs. 3–8 contain information on the rotational state distribution of $HCl(v' = 0)$ and $DCl(v' = 0)$, which should be very sensitive to the interatomic torques during the collision and hence provides a critical test of the PES. The j' rotational distributions for each initial j level of H_2 and D_2 were found in both QCT and QM calculations to not vary greatly with scattering angle, as shown in Fig. 15 for $Cl + H_2$ at $E_c = 5.85$ kcal mol^{-1}. They were converted into final relative translational energy distributions, $P_j(E)$, and then to CM speed distributions, $P_j(u)$, for each initial j of H_2 and D_2, with $P_j(u)$ treated as a continuous function. The CM flux for $HCl(v' = 0)$ and $DCl(v' = 0)$ has been obtained according to:

$$I_{CM}(\theta, u) = \sum_{j=0,\,1,\,2,\,3} w_j T_j(\theta) P_j(u) \tag{19}$$

where w_j are the relative weights of the H_2 or D_2 rotational levels in the beam, the $T_j(\theta)$ functions are the calculated CM DCS for each initial j of H_2 or D_2 summed over all j' (as shown in Figs. 13 and 19(a)), and the $P_j(u)$ functions are obtained from the rotational distributions of Figs. 14 and 19(b) as discussed above. The CM DCS for each initial j is transformed into the LAB frame using the appropriate Jacobian and averaged over the finite resolution of experimental conditions, taking into account the strong energy dependence of the reactive integral cross section.

The curves reported in Figs. 3–8 along with the experimental distributions were obtained as follows:

(a) for the $Cl + H_2$ experiment, we have used the QM DCSs derived for the different initial j of H_2 at a constant collision energy of 5.85 kcal mol^{-1}; because of the experimental collision energy spread, the QM collision energy dependence of the integral cross section for $j = 1$ (see Fig. 10), whose contribution to reactive scattering is dominant, was included in the simulation;

(b) for the $Cl + D_2$ experiment, we have used the QCT DCSs derived for the different initial j of D_2 at a constant collision energy of 6.4 kcal mol^{-1} shown in Fig. 19; in this case the QM calculations were performed only at a constant total energy of 10.6 kcal mol^{-1} (see Table 1). However, since QCT DCSs at the same collision energies for the various initial j of D_2 show generally good agreement with the QM ones (see Figs. 16 and 17), the use of QCT results for the laboratory simulations is warranted (QM results are expected to give predictions in the LAB frame which are indistinguishable from the QCT ones). The energy dependence of the integral cross section was also considered in this case as obtained from QCT calculations.[17]

Consider first the $Cl + H_2$ reaction. The QM results, averaged over experimental conditions as outlined above, are compared with the experimental data in Figs. 3 and 6. These figures show quite good agreement between the calculated and experimental total LAB angular and TOF distributions (a similar comparison has been performed between the QCT results and experiment;[3] once averaged over the experimental conditions, the LAB distributions generated starting from QCT CM functions are indistinguishable from those generated from QM functions, as expected from the close similarity between QM and QCT results especially for $j = 1$ of H_2, which is the dominant contribution). The sharp peaking of the LAB angular distribution in the backward direction is well reproduced by theory (see Fig. 3), which predicts the CM DCS to be strongly backward (Fig. 13). Both QM and QCT calculations indicate that ~80% of the total available energy in the CM frame is deposited into translation; hence, by energy conservation, the remaining 20% goes into product rotation. The theoretical calculations predict very little variation of the

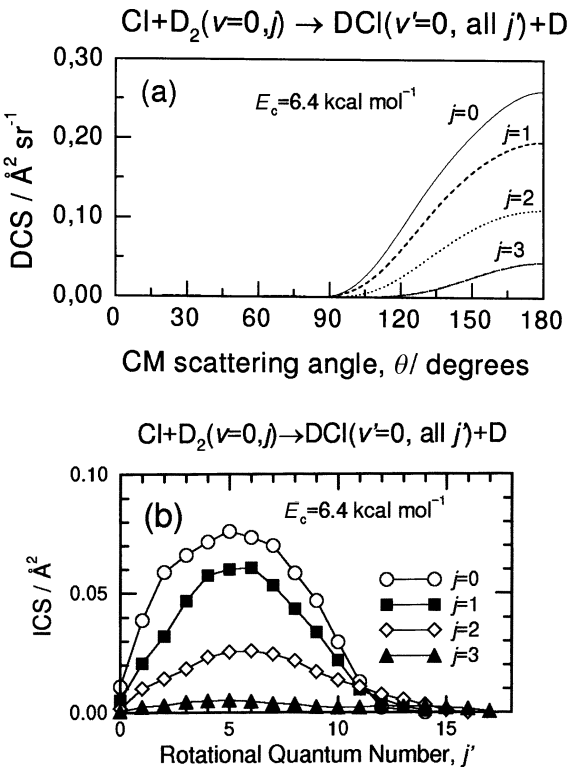

Fig. 19 (a) QCT differential cross sections for the $Cl + D_2(v = 0,\ j = 0, 1, 2, 3) \rightarrow DCl(v' = 0) + D$ reaction at the collision energy $E_c =$ 6.4 kcal mol^{-1}, and (b) integral cross sections as a function of the final rotational state j' of $DCl(v' = 0)$.

product rotational excitation with the scattering angle, and this is in line with experiment. Indeed, the TOF data are quite well reproduced (Fig. 6) by using the same rotational distribution (that is, the same translational energy distribution) in all angular range of the CM DCS. Even though the general shape and main features of the LAB angular and TOF distributions are quite well reproduced by theory, small discrepancies, which are not within the experimental error, are visible. The experimental angular distribution is broader; in particular, the maximum is less sharp and the intensity of the tail at large angles (on the right side of the CM angle, Θ_{CM}) is higher than that of the QM (and also QCT) prediction (*cf.* Fig. 3). The slow side of the TOF distributions is also not well predicted, with a substantial underestimate of the intensity of slow products at all angles (see Fig. 6).

In the case of $Cl + D_2$, the agreement between experiment and theory is less satisfactory, and the small deviations noted for $Cl + H_2$ become more significant, especially in the case of the experiment at $E_c = 6.4$ kcal mol^{-1} where the favourable kinematics helps in revealing them. The LAB angular distributions derived from the QCT functions are lower than experiment for sideways scattering (*i.e.*, near Θ_{CM}, see Figs. 4 and 5), and the small angle TOF spectra are somewhat faster than the experimental ones (see Figs. 7 and 8).

What is the source of the observed discrepancies? One possibility is that the QM and QCT calculations on the G3 PES substantially underestimate the reactivity of rotationally excited reactants (initial $j > 0$); an increase of reactivity for $j = 1$, 2 would lead to a significant improvement in the fit of the experimental data at large angles. However, this would not be enough, especially in the case of $Cl + D_2$. The strong collision energy dependence of the integral cross sections has the effect of cutting out the low collision energy contributions to the observed signals; as a matter of fact, the most significant improvement in the fit of the experimental data can be obtained by shifting the reaction threshold, so that lower collision energy Newton diagrams can contribute in the simulation. In any case, the larger cross sections for the reaction with initial $j = 1$ in comparison to $j = 0$ found experimentally by Lee *et al.*[10] for the $Cl + H_2$ reaction, in contrast with the present theoretical predictions on the G3 PES, and the somewhat smaller reaction threshold found by these authors, would help to account for our LAB angular distributions and TOF spectra.

Another possibility is the contribution to reaction from $Cl(^2P_{1/2})$ atoms, also present in the beam, through nonadiabatic channels. If the spin–orbit energy content were efficiently channelled into relative translational energy in the entrance channel of the reaction, there would be 2.52 kcal mol^{-1} extra energy available. The effect would be a shift in the threshold of the integral cross section to lower energy values and it might improve the significant disagreement of theory and experiment for small LAB scattering angles also because the higher translational energies lead to more sideways scattering. In a recent paper by Lee and Liu,[11] spin–orbit effects on the $Cl(^2P) + H_2$ reaction have been investigated in a crossed molecular beam experiment by exploiting two different sources for the generation of $Cl(^2P)$ beams. Surprisingly, these authors estimated from their Doppler-selected TOF measurements that the spin–orbit excited $Cl(^2P_{1/2})$ atoms were more reactive with H_2 molecules at $E_c = 5.2$ kcal mol^{-1} than the ground $Cl(^2P_{3/2})$ atoms by, at least, a factor of 5. In addition, they found that for the ground spin–orbit state reaction, the HCl product appeared translationally hot with only about 12% of the available energy disposed into rotation, the j' distribution being relatively narrow (peaking at $j' \approx 4$–5) and the DCS peaking at 180°. However, the HCl produced from the $Cl(^2P_{1/2})$ reaction appeared rotationally hotter, with the rotational distribution peaking at $j' \approx 9$ and the contribution of large j' values to the total, strongly backward, DCS was more in the sideways scattering region.

In conclusion, although the main features of the scattering results for the title reactions are for the most part well predicted by theory, some discrepancies remain. These discrepancies may have a similar origin as the discrepancies observed by Liu and co-workers[11] in other recent experiments. First of all, it seems that those parts of the ground-state potential energy surface that control rotational energy utilization and disposal, for example the anisotropy and bending potential, may require further quantitative refinement. Secondly, the agreement would be improved if there is a significant contribution of nonadiabatic reaction, and it is important to gain a better understanding of the possible participation of nonadiabatic processes (the dynamical coupling of the excited spin–orbit state of Cl to the ground state) in the observed signal. Electronically nonadiabatic reactive scattering calculations are now feasible for three-body systems,[63–65] but only in the case of the $F + H_2$ reaction have they been combined with accurate potential energy surfaces and couplings;[65] extending such studies to the $Cl + H_2$ reaction would be valuable.

VI. Concluding remarks

Experimental laboratory angular distributions and time-of-flight spectra have been measured for the $Cl + H_2$ and $Cl + D_2$ reactions using a universal crossed molecular beam apparatus. Quantal and quasiclassical trajectory calculations have been carried out for the two isotopic variants on the G3 PES at a series of collision energies and initial rotational states, in order to obtain reaction probabilities as a function of total energy for $J = 0$, and the energy dependence of the integral cross section and differential cross sections.

The most significant differences between QM and QCT results are found at low collision energies in the vicinity of the effective reaction threshold. For initial $j = 0$ the QCT cross sections are larger than the QM ones, whereas at $j = 1$ and, especially, at $j = 2$ the opposite situation takes place. The shapes of the vibrationally resolved DCS are similar in the two cases.

The general features of the experimental LAB angular distributions and TOF spectra can be simulated well using either the QM or QCT results. However, a detailed inspection shows some significant discrepancies between experiment and theory which could be attributed to a larger reactivity as initial j increases, just the opposite behaviour than that obtained in the present QM/QCT calculations on the G3 PES, and/or to the participation in the reaction of spin–orbit excited $Cl(^2P_{1/2})$ atoms, present in our beam.

Acknowledgements

We dedicate this paper to the memory of Roger Grice. He has been one of the leading practitioners of the "crossed molecular beams" technique; his work has been of great inspiration to many of us and has contributed to deepening our understanding of the dynamics of elementary chemical reactions. The authors are grateful to David W. Schwenke for assistance with some of the calculations, and to Eddy H. van Kleef for his help during the early stages of the experiments. This work was supported, in part, by the Italian "Consiglio Nazionale delle Ricerche" (CNR) and "Ministero Università e Ricerca Scientifica" (MURST-COFIN 97), by the Spanish D.G.I.C.Y.T. grant no. PB95-0918-C03-01 and PB98-0762-C03-01, and by grant No. CHE97-25965 from the U.S. National Science Foundation.

Note added in proof

A new, fully *ab initio* PES for ClH_2 has recently been published[66] as well as a semiempirical surface obtained by

scaling the *ab initio* correlation energy using the SEC method.[67] The semiempirical surface has saddle point properties very similar to the G3 surface but a wider barrier. It will be interesting in the future to compare the prediction of the new PESs with the present scattering results.

References

1 T. C. Allison, S. L. Mielke, D. W. Schwenke, G. C. Lynch, M. S. Gordon and D. G. Truhlar, in *Gas-Phase Reaction Systems: experiments and models 100 years after Max Bodenstein*, ed. J. Wolfrum, H.-R. Volpp, R. Rannacher and J. Warnatz, Springer, Heidelberg, 1996, p. 111.
2 M. Alagia, N. Balucani, P. Casavecchia, D. Stranges and G. G. Volpi, *J. Chem. Soc., Faraday Trans.*, 1995, **91**, 575.
3 M. Alagia, N. Balucani, L. Cartechini, P. Casavecchia, E. H. Van Kleef, G. G. Volpi, F. J. Aoiz, L. Bañares, D. W. Schwenke, T. C. Allison, S. L. Mielke and D. G. Truhlar, *Science*, 1996, **273**, 1519.
4 M. Zhao, M. Mladenovic, D. G. Truhlar, D. W. Schwenke, Y. Sun, D. J. Kouri and N. C. Blais, *J. Am. Chem. Soc.*, 1989, **111**, 852; N. C. Blais, M. Zhao, M. Mladenovic, D. G. Truhlar, D. W. Schwenke, Y. Sun and D. J. Kouri, *J. Chem. Phys.*, 1989, **91**, 1038; F. J. Aoiz, L. Bañares and V. J. Herrero, in *Advances in Classical Trajectory Methods. Comparisons of classical and quantum dynamics*, ed. W. Hase, JAI Press, Stanford, 1998, vol. 3, p. 121, and references therein.
5 F. J. Aoiz, L. Bañares and V. J. Herrero, *J. Chem. Soc., Faraday Trans.*, 1998, **94**, 2483.
6 P. Casavecchia, N. Balucani and G. G. Volpi, *Annu. Rev. Phys. Chem.*, 1999, **50**, 347.
7 (*a*) D. L. Chapman and L. K. Underhill, *J. Chem. Soc.*, 1913, 496; (*b*) M. Bodenstein and W. Dux, *Z. Phys. Chem. (Leipzig)*, 1913, **85**, 297; (*c*) W. Nernst, *Z. Elektrochem.*, 1918, **24**, 335; (*d*) M. Bodenstein, *Z. Elektrochem.*, 1913, **85**, 329; (*e*) M. Bodenstein, *Z. Elektrochem.*, 1916, **22**, 53.
8 H. Eyring and M. Polanyi, *Z. Phys. Chem (Leipzig) B*, 1931, **12**, 279; J. O. Hirschfelder, H. Eyring and B. Topley, *J. Chem. Phys.*, 1936, **4**, 170; A. Wheeler, B. Topley and H. Eyring, *J. Chem. Phys.*, 1936, **4**, 178; S. Sato, *J. Chem. Phys.*, 1955, **23**, 2465; K. J. Laidler, *Chemical Kinetics*, Harper & Row, New York, 3rd edn., 1987, pp. 14, 288–298.
9 S. S. Kumaran, K. P. Lim and J. V. Michael, *J. Chem. Phys.*, 1994, **101**, 9487.
10 S.-H. Lee, L.-H. Lai and K. Liu, *J. Chem. Phys.*, 1999, **110**, 8229.
11 S.-H. Lee and K. Liu, *J. Chem. Phys.*, 1999, **111**, 6253.
12 T. C. Allison, G. C. Lynch, D. G. Truhlar and M. S. Gordon, *J. Phys. Chem.*, 1996, **100**, 13575.
13 D. W. Schwenke, S. C. Tucker, R. Steckler, F. B. Brown, G. C. Lynch, D. G. Truhlar and B. C. Garrett, *J. Chem. Phys.*, 1989, **90**, 3110.
14 M. J. Stern, A. Persky and F. S. Klein, *J. Chem. Phys.*, 1973, **58**, 5697.
15 S. L. Mielke, T. C. Allison, D. G. Truhlar and D. W. Schwenke, *J. Phys. Chem.*, 1996, **100**, 13588.
16 H. Wang, W. H. Thompson and W. H. Miller, *J. Chem. Phys.*, 1997, **107**, 7194.
17 F. J. Aoiz and L. Bañares, *J. Phys. Chem.*, 1996, **100**, 18108.
18 F. J. Aoiz and L. Bañares, *Chem. Phys. Lett.*, 1995, **247**, 232.
19 D. C. Chatfield, R. S. Friedman, S. L. Mielke, D. W. Schwenke, G. C. Lynch, T. C. Allison and D. G. Truhlar, in *Dynamics of Molecules and Chemical Reactions*, ed. R. E. Wyatt and J. Z. H. Zhang, Dekker, New York, 1996, p. 323; J. Srinivasan, T. C. Allison, D. W. Schwenke and D. G. Truhlar, *J. Phys. Chem. A*, 1999, **103**, 1487.
20 C. A. Taatjes, *Chem. Phys. Lett.*, 1999, **306**, 33.
21 (*a*) R. A. Brownsword, C. Kappel, P. Schmiechen, H. P. Upadhyaya and H.-R. Volpp, *Chem. Phys. Lett.*, 1998, **289**, 241; (*b*) V. J. Barclay, B. A. Collings, J. C. Polanyi and J. H. Wang, *J. Phys. Chem.*, 1991, **95**, 2921; (*c*) P. A. Aker, G. J. German and J. J. Valentini, *J. Chem. Phys.*, 1989, **90**, 4795.
22 J. M. Launay and S. B. Padkjaer, *Chem. Phys. Lett.*, 1991, **181**, 95.
23 S. E. Branchett, S. B. Padkjaer and J. M. Launay, *Chem. Phys. Lett.*, 1993, **208**, 523.
24 S. Takada, K.-I. Tsuda, A. Ohsaki and H. Nakamura, in *Advances in Molecular Vibrations and Collision Dynamics*, ed. J. M. Bowman, JAI Press, Greenwich, 1994, vol. 2A, pp. 245–284.
25 P. Casavecchia, *Rep. Prog. Phys.*, 2000, in the press.
26 S. J. Sibener, R. J. Buss, C. Y. Ng and Y. T. Lee, *Rev. Sci. Instrum.*, 1980, **51**, 167.
27 J. E. Pollard, D. J. Trevor, Y. T. Lee and D. A. Shirley, *J. Chem. Phys.*, 1982, **77**, 4818.
28 M. Alagia, V. Aquilanti, D. Ascenzi, N. Balucani, D. Cappelletti, L. Cartechini, P. Casavecchia, F. Pirani, G. Sanchini and G. G. Volpi, *Isr. J. Chem.*, 1997, **37**, 329.
29 (*a*) W. B. Chapman, B. W. Blackman, S. A. Nizkorodov and D. J. Nesbitt, *J. Chem. Phys.*, 1998, **109**, 9306; (*b*) S. A. Nizkorodov, W. W. Harper and D. J. Nesbitt, *Faraday Discuss., Chem. Soc.*, 1999, **113**, 107; (*c*) S. A. Nizkorodov, W. W. Harper, W. B. Chapman, B. W. Blackman and D. J. Nesbitt, *J. Chem. Phys.*, 1999, **111**, 8404.
30 S. L. Mielke, D. G. Truhlar and D. W. Schwenke, *J. Chem. Phys.*, 1991, **95**, 5930.
31 Y. Sun, D. J. Kouri, D. G. Truhlar and D. W. Schwenke, *Phys. Rev. A*, 1990, **41**, 4857.
32 Y. Sun, D. J. Kouri and D. G. Truhlar, *Nuclear Phys. A*, 1990, **508**, 41c.
33 D. W. Schwenke, S. L. Mielke and D. G. Truhlar, *Theor. Chim. Acta*, 1991, **79**, 241.
34 Y. Sun and D. J. Kouri, *Chem. Phys. Lett.*, 1991, **179**, 142.
35 J. Z. H. Zhang, D. J. Kouri, K. Haug, D. W. Schwenke, Y. Shima and D. G. Truhlar, *J. Chem. Phys.*, 1988, **88**, 2492.
36 G. J. Tawa, S. L. Mielke, D. G. Truhlar and D. W. Schwenke, *J. Chem. Phys.*, 1994, **100**, 5751.
37 G. J. Tawa, S. L. Mielke, D. G. Truhlar and D. W. Schwenke in *Advances in Molecular Vibrations and Collision Dynamics*, ed. J. M. Bowman, JAI Press, Greenwich, 1994, vol. 2B, p. 45.
38 D. W. Schwenke, K. Haug, M. Zhao, D. G. Truhlar, Y. Sun, J. Z. H. Zhang and D. J. Kouri, *J. Phys. Chem.*, 1988, **92**, 3202.
39 M. Zhao, D. G. Truhlar, D. W. Schwenke and D. J. Kouri, *J. Phys. Chem.*, 1990, **94**, 7074.
40 S. L. Mielke, G. C. Lynch, D. G. Truhlar, D. W. Schwenke, *Chem. Phys. Lett.*, 1993, **213**, 10; *erratum*, 1994, **217**, 173.
41 S. L. Mielke, D. G. Truhlar and D. W. Schwenke, *J. Phys. Chem.*, 1994, **98**, 1053.
42 J. F. Castillo, D. E. Manolopoulos, K. Stark and H.-J. Werner, *J. Chem. Phys.*, 1996, **104**, 6531.
43 B. Martínez-Haya, F. J. Aoiz, L. Bañares, P. Honvault and J.-M. Launay, *Phys. Chem. Chem. Phys.*, 1999, **1**, 3415.
44 J.-M. Launay, *J. Phys. B*, 1976, **9**, 1823.
45 D. W. Schwenke, M. Mladenovic, M. Zhao, D. G. Truhlar, Y. Sun and D. J. Kouri, in *Supercomputer Algorithms for Reactivity, Dynamics, and Kinetics of Small Molecules*, ed. A. Laganà, Kluwer, Dordrecht, 1989, vol. 277, p. 131.
46 W. H. Miller and B. M. D. D. Jansen op de Haar, *J. Chem. Phys.*, 1987, **86**, 6213.
47 D. W. Schwenke and D. G. Truhlar, in *Computing Methods in Applied Sciences and Engineering*, ed. R. Glowinski and A. Lichnewski, Society for Industrial and Applied Mathematics, Philadelphia, 1990, p. 291.
48 J.-M. Launay and M. Le Dourneuf, *Chem. Phys. Lett.*, 1989, **163**, 178.
49 J. Z. H. Zhang, *J. Chem. Phys.*, 1991, **94**, 6047.
50 D. G. Truhlar and J. T. Muckerman, in *Atom–Molecule Collision Theory: A Guide for the Experimentalist*, ed. R. B. Bernstein, Plenum Press, New York, 1979, p. 505.
51 F. J. Aoiz, V. J. Herrero and V. Sáez Rábanos, *J. Chem. Phys.*, 1992, **97**, 7423.
52 N. C. Blais and D. G. Truhlar, *J. Chem. Phys.*, 1977, **67**, 1532.
53 N. C. Blais and D. G. Truhlar, *J. Chem. Phys.*, 1977, **67**, 1540.
54 F. J. Aoiz, L. Bañares, T. Díez-Rojo, V. J. Herrero and V. Sáez Rábanos, *J. Phys. Chem.*, 1996, **100**, 4071.
55 F. J. Aoiz, L. Bañares, V. J. Herrero, V. Sáez Rábanos and I. Tanarro, *J. Phys. Chem. A*, 1997, **101**, 6165.
56 (*a*) D. G. Truhlar, *J. Chem. Phys.*, 1972, **56**, 3189; (*b*) D. G. Truhlar, *J. Chem. Phys.*, 1974, **61**, 440(E).
57 F. J. Aoiz, H. K. Buchenau, V. J. Herrero and V. Sáez Rábanos, *J. Chem. Phys.*, 1994, **100**, 2789.
58 D. G. Truhlar and D. A. Dixon, in *Atom–Molecule Collision Theory: A Guide for the Experimentalist*, ed. R. B. Bernstein, Plenum Press, New York, 1979, p. 595; N. N. Sathyamurthy, *Chem. Rev.*, 1983, **83**, 601.
59 (*a*) J.-B. Song and E. A. Gislason, *J. Chem. Phys.*, 1995, **103**, 8884; (*b*) J.-B. Song and E. A. Gislason, *Chem. Phys.*, 1998, **237**, 159.
60 D. C. Chatfield, R. S. Friedman, D. W. Schwenke and D. G. Truhlar, *J. Phys. Chem.*, 1992, **96**, 2414.
61 F. J. Aoiz, V. J. Herrero, O. Puentedura and V. Sáez Rábanos, *Chem. Phys. Lett.*, 1992, **198**, 321.
62 S. L. Mielke, D. G. Truhlar and D. W. Schwenke, *J. Phys. Chem.*, 1994, **98**, 1053.
63 (*a*) S. L. Mielke, G. J. Tawa, D. G. Truhlar and D. W. Schwenke, *Chem. Phys. Lett.*, 1995, **234**, 57; (*b*) S. L. Mielke, D. G. Truhlar

and D. W. Schwenke, *J. Phys. Chem.*, 1995, **99**, 16210; (*c*) Y. L. Volobuev, M. D. Hack and D. G. Truhlar, *J. Phys. Chem. A*, 1999, **103**, 6225.
64 K. Drukker and G. C. Schatz, *J. Chem. Phys.*, 1999, **111**, 2451.
65 M. H. Alexander, H.-J. Werner and D. E. Manolopoulos, *J. Chem. Phys.*, 1998, **109**, 5710. See also: V. Aquilanti, S. Cavalli, D. De Fazio, A. Volpi, A. Aguilar, X. Gimenez and J. M. Lucas, *J. Chem. Phys.*, 1998, **109**, 3805
66 W. Bian and H.-J. Werner, *J. Chem. Phys.*, 2000, **112**, 220.
67 U. Manthe, W. Bian and H.-J. Werner, *Chem. Phys. Lett.*, 1999, **313**, 647.

Paper a908829f